LETTERS
PUBLISHED ONLINE: 11 APRIL 2010 | DOI: 10.1038/NNANO.2010.57
nature nanotechnology

Biologically templated photocatalytic nanostructures for sustained light-driven water oxidation

Yoon Sung Nam[1], Andrew P. Magyar[2], Daeyeon Lee[3], Jin-Woong Kim[3], Dong Soo Yun[2], Heechul Park[2], Thomas S. Pollom Jr[1], David A. Weitz[3,4] and Angela M. Belcher[1,2]*

Over several billion years, cyanobacteria and plants have evolved highly organized photosynthetic systems to shuttle both electronic and chemical species for the efficient oxidation of water[1]. In a similar manner to reaction centres in natural photosystems, molecular[2] and metal oxide[3] catalysts have been used to photochemically oxidize water. However, the various approaches involving the molecular design of ligands[4], surface modification[5] and immobilization[6,7] still have limitations in terms of catalytic efficiency and sustainability. Here, we demonstrate a biologically templated nanostructure for visible light-driven water oxidation that uses a genetically engineered M13 virus scaffold to mediate the co-assembly of zinc porphyrins (photosensitizer) and iridium oxide hydrosol clusters (catalyst). Porous polymer microgels are used as an immobilization matrix to improve the structural durability of the assembled nanostructures and to allow the materials to be recycled. Our results suggest that the biotemplated nanoscale assembly of functional components is a promising route to significantly improved photocatalytic water-splitting systems.

One of the most fascinating aspects of natural photosynthesis is the sophisticated self-organization of light-harvesting complexes, electron-transfer mediators and oxygen-evolving complexes[1]. In such photosystems, dozens of chlorophyll molecules within the light-harvesting complex are responsible for the primary light absorption event. This energy is efficiently transferred to the reaction centre, where it is transformed into a pair of spatially separated charge carriers. Sunlight-driven water splitting for hydrogen generation has received increasing attention as a means of storing solar energy in chemical bonds[8,9]. However, to evolve hydrogen efficiently in a sustainable manner, it is necessary first to develop a stable and efficient catalytic system for water oxidation, which is the more challenging half reaction of photo-driven water splitting[10–13]. The many attempts to model water-oxidation systems on photosynthesis have had limited success; most catalysts based on Mn-oxo need oxygen-transfer oxidants to catalyse oxygen formation[14]. Until now, the most promising catalytic systems have been based on metal oxide colloids, which drive the photochemical oxidation of water with several different components operating cooperatively: a photosensitizer absorbs visible light and subsequently transfers an electron to an electron acceptor, stimulating the transfer of a hole from the photosensitizer to the catalyst[15]. Repeated cycles of light absorption lead to the accumulation of four holes in the catalyst, and the holes drive the evolution of a molecule of oxygen from water. As in photosynthesis, the distances between the functional components are critically important in these colloidal systems; non-optimal spacing between the photosensitizer, electron acceptor and catalyst can kinetically promote corrosive mechanisms, leading to the degradation of catalytic materials[16].

Various approaches to develop efficient sustainable metal oxide catalysts driven by visible light have been undertaken, including the polyelectrolyte-mediated complexation of catalysts and photosensitizers[17], ligand design[5] and the development of heterogeneous catalysts[3,7]. However, it is challenging to design multicomponent systems with controlled structural arrangement at the molecular level. A lack of this precise arrangement can hinder the appropriate trafficking of chemical and electron species between individual active components[5]. Polymers are often used as intermediate binders to couple photosensitizers to the surface of metal oxide catalysts[7,17]. These polymers, however, often undergo undesirable conformational variations during charge building and the subsequent chemical reactions. These structural changes can affect the distances between and relative orientations of catalysts and photosensitizers, which in turn greatly affect charge transfer kinetics[18]. Therefore, to formulate efficient, sustainable photochemical water-splitting systems, structurally stable and controllable microenvironments that can coordinate complicated electrochemical events are required.

Unique multiscale structures of natural photosystems, which have evolved to efficiently handle complex photochemical processes, motivated us to investigate the use of biological scaffolds to spatially organize multiple functional materials for photochemical water splitting. A virus can serve as a versatile template for the assembly of various materials through both genetically controllable biomineralization[19–21] and chemical linkage[22]. In this study, photosensitizers and metal oxide catalysts were co-assembled in close proximity on M13 virus scaffolds to create a photocatalytic nanostructure. Iridium oxide (IrO_2) was chosen as a water-oxidation catalyst because of its well-known catalytic activity and stability under oxidizing conditions[3,5,16]. M13 viruses carrying the IrO_2 binding peptide, AGETQQAM, on the major coat protein were identified through biopanning against IrO_2 using an M13 library displaying random octameric peptides[23]. These engineered M13 viruses were successfully used as templates for the self-assembly of IrO_2 nanoscale structures (Supplementary Fig. S7).

As a photosensitizer, Zn(II) deuteroporphyrin IX 2,4 *bis*-ethylene glycol (ZnDPEG) was selected for its optical and electrochemical properties as well as its functional groups (Supplementary Fig. S1). ZnDPEG was chemically grafted to the M13 major coat proteins via a carbodiimide reaction. M13 virus has ~2,700 copies of α-helical major coat proteins, which are highly ordered on the viral DNA[24]. Every coat protein has two primary amines (*N*-terminus

[1]Department of Biological Engineering, Massachusetts Institute of Technology, Cambridge, Massachusetts 02139, USA, [2]Department of Materials Science and Engineering, Massachusetts Institute of Technology, Cambridge, Massachusetts 02139, USA, [3]School of Engineering and Applied Sciences, Harvard University, Cambridge, Massachusetts 02138, USA, [4]Department of Physics, Harvard University, Cambridge, Massachusetts 02138, USA.
*e-mail: belcher@mit.edu

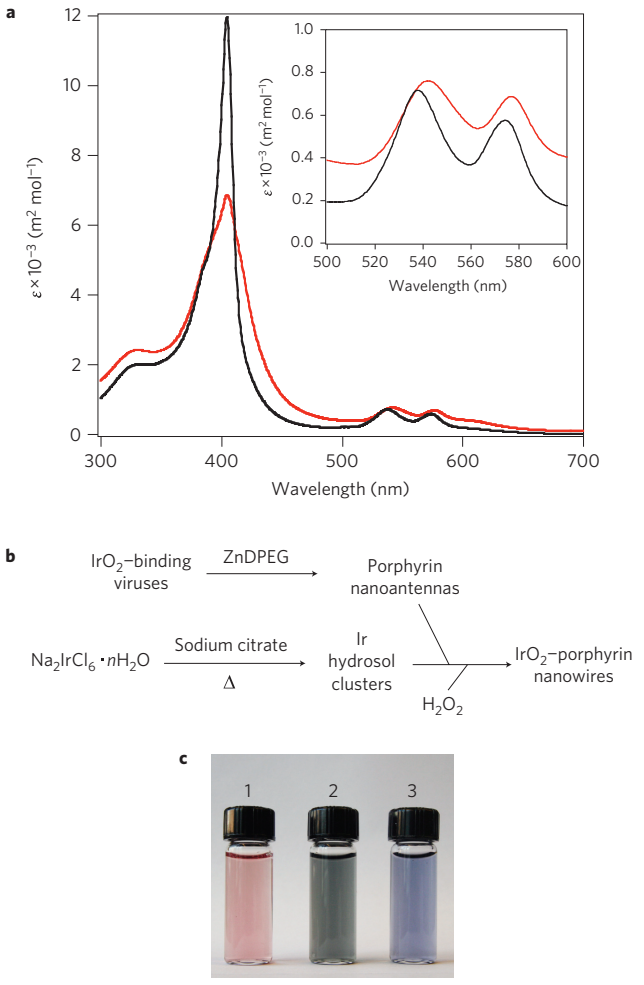

Figure 1 | Synthesis of IrO_2–porphyrin nanowires. a, Absorption spectra of porphyrins (black) and ZnDPEG-conjugated viruses (red). The *y* axis denotes the molar extinction coefficient ε. Inset: magnification of the Q-band region. **b**, Schematic synthetic routes for IrO_2–porphyrin nanowires. **c**, Digital camera images of aqueous solutions of ZnDPEG (1), IrO_2–ZnDPEG nanowires (2) and IrO_2 nanowires (3).

and lysine) exposed on the virus surface. Inductively coupled plasma–atomic emission spectrometry (ICP–AES) analysis indicated that the molar ratio of zinc to phosphorus was 0.39:1, which corresponds to about 2,730 porphyrins per virus. The absorption spectrum of ZnDPEG in water shows a strong Soret band at 406 nm and weak Q-bands at 538 and 574 nm (Fig. 1a). The conjugation of ZnDPEG to M13 viruses resulted in a significant broadening of the Soret band and a redshift of the Q-bands (Fig. 1a, inset). Furthermore, the fluorescence of the conjugated ZnDPEG was dramatically suppressed compared to that of unconjugated ZnDPEG (Supplementary Fig. S2)[25]. These spectral changes suggest that the close proximity of neighbouring porphyrins on the virus induces excitonic migration, as shown with ZnDPEG conjugated to the wild-type M13 virus[26,27].

To co-immobilize IrO_2 and ZnDPEG on the virus, aqueous sodium hexachloroiridate was hydrolysed with citrate as a ligand[16] and self-assembled into IrO_2–ZnDPEG core–shell nanowires by incubation with the ZnDPEG-conjugated M13 viruses at room temperature (Fig. 1b). As a control, IrO_2 hydrosol clusters were synthesized without the virus templates (Supplementary Fig. S3). The IrO_2–ZnDPEG core–shell nanowires were dark green, but the ZnDPEG and IrO_2 nanowires were red and blue, respectively (Fig. 1c).

The IrO_2 shell thickness of the IrO_2–ZnDPEG nanowires was controlled by varying the amount of hydrated IrO_2 clusters while fixing the number of ZnDPEG-conjugated viruses for mineralization. The IrO_2:ZnDPEG molar ratio, denoted by *r*, was determined by ICP-AES quantification of iridium and zinc. Figure 2 shows the transmission electron micrographs (TEM) of the ZnDPEG-conjugated M13 viruses (Fig. 2a) and the IrO_2–ZnDPEG nanowires with different IrO_2 shell thicknesses, $r = 15$ (Fig. 2b) and $r = 224$ (Fig. 2c). The prepared IrO_2 nanowires were hydrated such that $x \approx 2$ in $IrO_2 \cdot xH_2O$, as determined by X-ray photoelectron spectroscopy (see Supplementary Information).

IrO_2 hydrosol clusters (32.7 μM) dispersed with unconjugated ZnDPEG (8 μM) at pH 11 showed a turnover number (TON), the total number of water molecules the catalyst splits, of ~180 (four times the amount of O_2 evolved per iridium atom; Fig. 3a). Their turnover rate (TOR), the number of water molecules the catalyst splits per unit time per surface active site, was ~0.27 s^{-1}. This TOR was calculated from the steady-state oxygen evolution rate with an assumption that 53% of the total iridium atoms were exposed to the surface of the catalyst (see Supplementary Information)[28]. These values are comparable with previously reported data from IrO_2 nanoparticles using different photosensitizers[7,28]. However, IrO_2 nanowires mixed with unconjugated ZnDPEGs demonstrated TON ≈ 76, only 44% that of the IrO_2 hydrosol clusters. This reduced TON seems to be attributable to the smaller surface area per mass (232 m^2 g^{-1}) when compared with IrO_2 hydrosol clusters[5]. As expected, the TOR (~0.07 s^{-1}) was similar to that of the IrO_2 hydrosol clusters. Interestingly, despite the small surface area, IrO_2–ZnDPEG nanowires assembled through the formation of an IrO_2 shell on the ZnDPEG-conjugated M13 core show dramatically higher water-splitting activities: TOR ≈ 0.85 s^{-1} and TON ≈ 790. This high activity seems to be a synergistic result of excitonic migration between photosensitizers and the close arrangement of the photosensitizers with IrO_2. To determine the effects of energy transfer on oxygen evolution, we tested IrO_2 hydrosol clusters with ZnDPEG-conjugated M13 not expressing the IrO_2 binding peptide, which resulted in TOR ≈ 0.35 s^{-1} and TON ≈ 310 (Fig. 3a). Both values were significantly higher than those of IrO_2 hydrosol clusters with unconjugated ZnDPEG. Moreover, the IrO_2 shell thickness turned out to be a critically important parameter for water oxidation activity, as shown in Fig. 3b. Both TON and TOR for IrO_2 increased with decreasing *r* with a highest TON of ~1,100 and TOR of ~1.68 s^{-1} at $r = 15$. To compare the water-oxidation rate relative to the decomposition rate of the oxidized photosensitizer, TON was also calculated in terms of the number of photosensitizers used. The value of TON for ZnDPEG increased with increasing *r* from TON ≈ 1.7×10^4 at $r = 15$ to TON ≈ 9.7×10^4 at $r = 224$, all significantly greater than the value for free IrO_2 nanoparticles mixed with free ZnDPEG (TON ≈ 7.4×10^3). These results indicate that the use of excess amount of catalyst can prolong the chemical stability of the photosensitizers, presumably because the generated charges can be more quickly transferred from the oxidized photosensitizer to the adjacent catalysts. The quantum yield (Φ) was also measured using monochromic radiation at 550 nm with a light intensity of 200 mW cm^{-2}. IrO_2–ZnDPEG nanowires had Φ ≈ 0.86 at $r = 15$ when a Rayleigh scattering approximation was assumed. This value is significantly higher than that of IrO_2 nanoparticles with free ZnDPEG: Φ ≈ 0.47. The higher Φ of the IrO_2–ZnDPEG nanowires clearly shows that the increased value of TON was not due to the greater number of photons absorbed by the composite nanowire system. Therefore, comparison of the systems in terms of both Φ and TON has demonstrated that appropriate co-assembly of catalysts with photosensitizers is an effective means by which to increase light conversion into chemical potential for water oxidation.

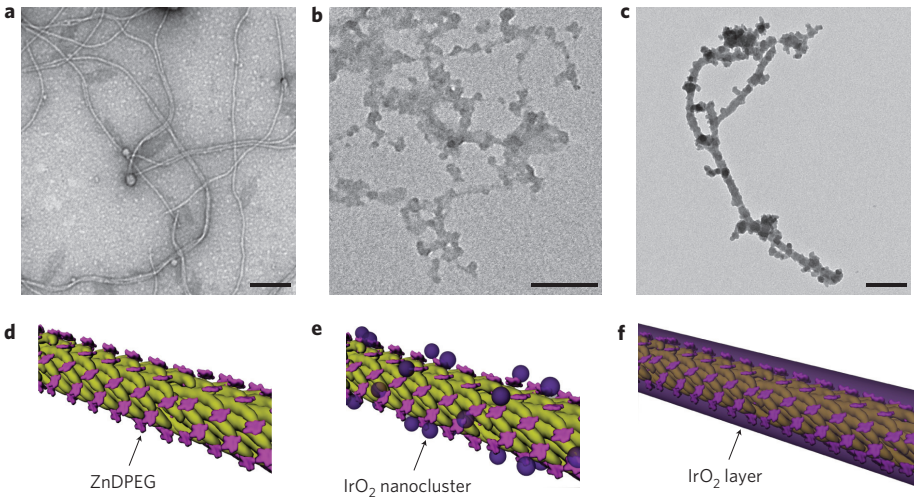

Figure 2 | Transmission electron micrographs of porphyrin and IrO_2–porphyrin nanowires. a–c, TEM images showing ZnDPEG nanoantennas after negative staining (**a**) and IrO_2–ZnDPEG hybrid nanowires at IrO_2:ZnDPEG molar ratios of $r = 15$ (**b**) and $r = 224$ (**c**). Scale bars, 200 nm. **d–f**, Each structure is schematically drawn using Protein Data Bank structure 2C0W.

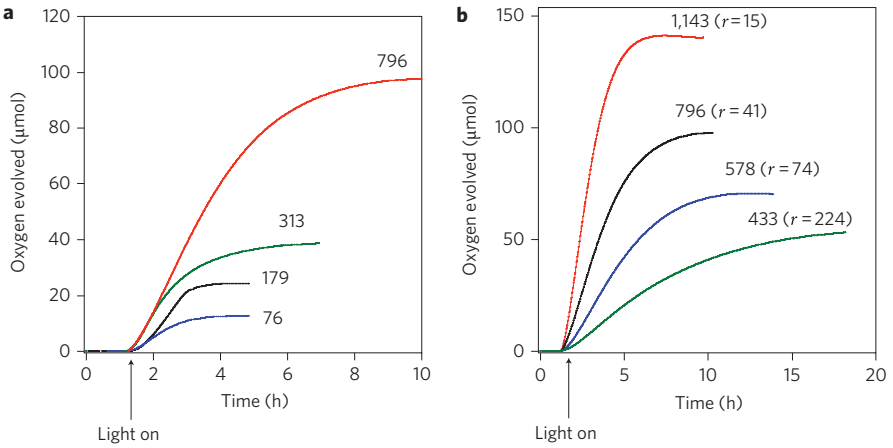

Figure 3 | Oxygen evolution from IrO_2–porphyrin nanowires. a, Time-course oxygen production profiles for IrO_2 hydrosol clusters mixed with unconjugated ZnDPEG (black), IrO_2 hydrosol clusters mixed with ZnDPEG-conjugated viruses (green), virus-templated IrO_2 nanowires mixed with unconjugated ZnDPEG (blue), and IrO_2–ZnDPEG hybrid nanowires (red). The concentrations of IrO_2 and ZnDPEG were fixed at 32.7 mM and 0.8 mM, respectively. **b**, Time-course oxygen production profiles for IrO_2–ZnDPEG hybrid nanowires having different ratios of IrO_2 to ZnDPEG: $r = 15$ (red), 41 (black), 74 (blue) and 224 (green). The numbers above the curves indicate TON values.

Photochemical colloidal catalysts are prone to aggregation[7], and this structural instability limits their practical applications. For instance, the IrO_2–ZnDPEG nanowires showed spontaneous precipitation after an oxygen evolution experiment (Supplementary Fig. S8). To eliminate nanowire aggregation, porous microgels were used as an immobilization matrix, maintaining the structural integrity of the IrO_2–ZnDPEG nanostructures. Using a microfluidic technique (Fig. 4a), monodisperse aqueous droplets incorporating the viruses and acrylic monomers were generated and subsequently converted to microgels (Fig. 4b) by initiating polymerization under ultraviolet irradiation[29]. The encapsulated viruses were homogeneously distributed within the microgels without any phase segregation, as confirmed by fluorescent labelling (Fig. 4b, inset). Viruses encapsulated in microgels were subsequently used as templates for assembling IrO_2 hydrosol clusters and photosensitizers. ZnDPEG was covalently attached to viruses in the microgel by pre-activating carboxylic acids groups of ZnDPEG with carbodiimides. After rigorous rinsing with water to remove loosely bound ZnDPEG, IrO_2 clusters were assembled on the viruses *in situ* by diffusion of hydrated iridium precursors into the microgels followed by chemical oxidation. Energy dispersive X-ray (EDX) analysis with scanning electron microscopy indicated the homogeneous distribution of iridium elements in the microgels (Fig. 4c,d). Two different IrO_2–ZnDPEG microgels were prepared with $r = 35$ and 109, as determined by ICP–AES analysis. As observed in the IrO_2–ZnDPEG nanowires, significantly more oxygen evolved from microgels having a lower IrO_2:ZnDPEG ratio, as shown in Fig. 4e. To demonstrate the recycling capability of the microgel-based system, oxygen evolution from the microgels was halted at 90 min post-illumination. The microgels were then collected through centrifugation and re-suspended in 0.2% hydrogen peroxide to re-oxidize the catalyst. The regenerated microgels showed ~94% oxygen evolution compared to the TON in the first cycle, and the value decreased to 56% in the fourth cycle (Fig. 4f). As a result, the cumulative TON after four reaction cycles became ~1.6 times higher than the TON of the full single reaction. These data demonstrate for the first time the recycling capability of a light-driven water-splitting system. However, deterioration of the catalytic activity

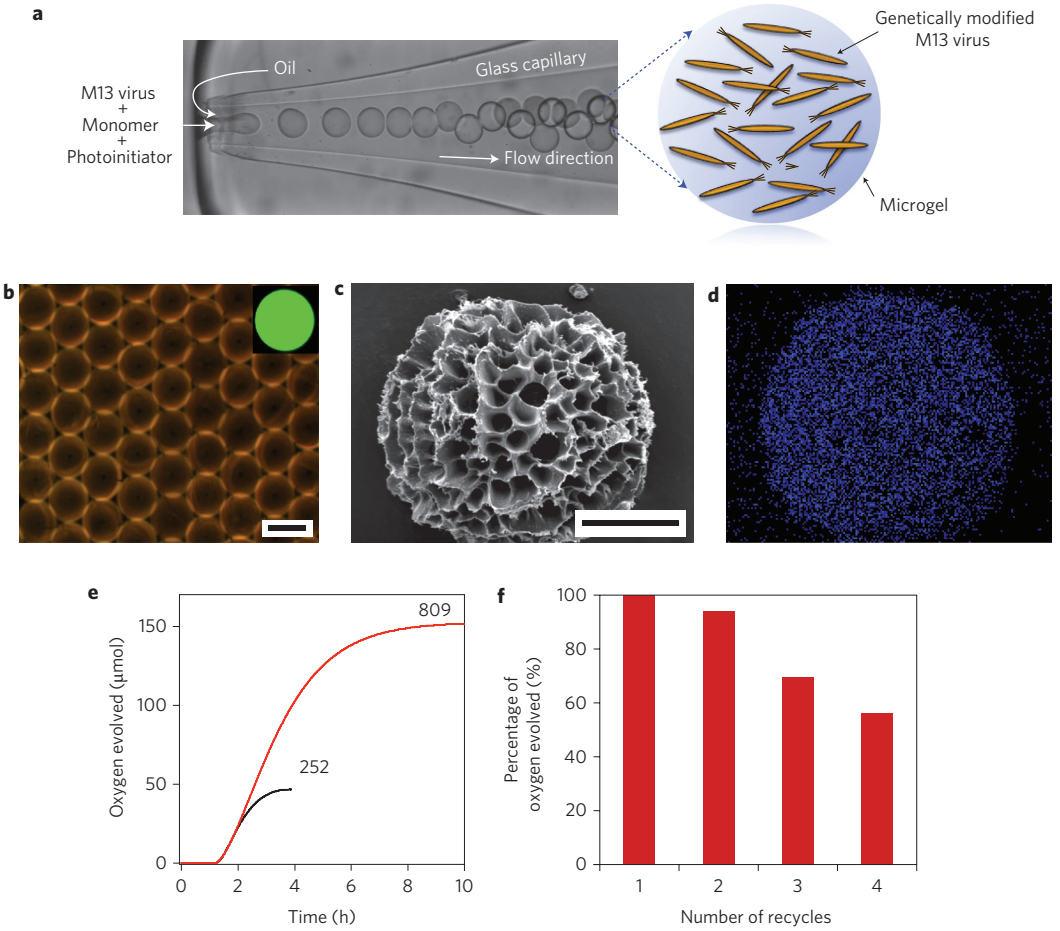

Figure 4 | Regeneration of catalytic materials. a, Injection part of the glass capillary device for fabrication of the virus-loaded microgels. **b**, Monodisperse virus-loaded microgels prepared from the microfluidic device. Scale bar, 100 μm. **c**,**d**, Scanning electron micrograph (**c**) and elemental map (**d**) of the freeze-dried microgel containing IrO_2–ZnDPEG nanostructures. Scale bar, 20 μm. Iridium is represented by blue dots. **e**, Oxygen evolution profiles from IrO_2–ZnDPEG microgels with $r = 35$ (black) and 109 (red). The numbers above the curves indicate TON values. **f**, Recycling efficiency of IrO_2–ZnDPEG microgels.

was consistently observed, presumably because of the photochemical degradation of the photosensitizers attached to the virus[30]. To improve the chemical stability of the system, our research is now directed towards further optimizing both the material properties and the reactor design. For instance, despite their high initial performance, the sacrificial electron acceptors used in this study may produce hydroxyl radicals, which seem to facilitate the degradation of photosensitizers. Their replacement with appropriate non-sacrificial materials or the coupling of the current system to a hydrogen-evolving catalyst may also reduce certain corrosive processes. We expect that, for a broad range of catalysts, a nanoscale architecture based on genetically modified biomaterials can offer a useful platform for multi-component photochemical devices, enabling the efficient, sustained production of clean fuels from sunlight.

Methods

To identify IrO_2-binding peptide sequences, we constructed a library of 1×10^{10} random octameric peptides displayed at the *N*-terminus of pVIII, the major coat protein[23]. After three rounds of biopanning against Ir(IV)O_2 powder (99.9%), M13 viruses carrying a dominant binding sequence, AGETQQAM, in each copy of pVIII were isolated and identified.

To synthesize the IrO_2 nanowires, aqueous sodium hexachloroiridate (Na_2IrCl_6) was hydrolysed to iridium hydrosols with citrate[16] and mixed with the viruses carrying AGETQQAM. The resulting iridium hydrosols were oxidized using 0.2% hydrogen peroxide. The solution was magnetically stirred while exposed to air at room temperature for at least one day and purged with nitrogen for 4 h before oxygen evolution measurement. Complete decomposition of residual hydrogen peroxide was confirmed by a fluorescent scopoletin assay using horseradish peroxidase (see Supplementary Information).

For the oxygen evolution studies, sodium borate was used as a proton acceptor and sodium persulphate was used as a sacrificial electron acceptor. The pH of the borate buffered solution was adjusted to pH 11 to optimize hole transfer from the ZnDPEG radical cations to IrO_2 catalyst[17]. The catalyst solution was purged with nitrogen as a carrier gas while illuminated with a 300 W xenon light source through a long wavelength pass filter (>400 nm). Oxygen evolution was continuously monitored using a ZrO_2-based gas analyser (Supplementary Fig. S4).

To produce monodisperse microgels, we fabricated a flow focusing glass capillary device consisting of a tapered cylindrical collection tube having an orifice 150 μm in diameter fitted in a square capillary[29]. Two immiscible fluids were infused into the device from opposite sides of the square capillary. The outer fluid (white mineral oil with 3 wt% Abil® EM90, Degussa) focuses the inner fluid (aqueous mixture of acrylamides, *bis*-acrylamides, 2-hydroxyl-2-methyl-1-phenyl-1-propanone and viruses) into the orifice of the collection tube and breaks the inner fluid into monodisperse droplets. Collected emulsions are converted to microgels by initiating polymerization using ultraviolet irradiation (365 nm, 3 W).

Received 30 October 2009; accepted 1 March 2010; published online 11 April 2010

References

1. Ferreira, K. N., Iverson, T. M., Maghlaoui, K., Barber, J. & Iwata, S. Architecture of the photosynthetic oxygen-evolving center. *Science* **303,** 1831–1838 (2004).
2. Gersten, S. W., Samuels, G. J. & Meyer, T. J. Catalytic-oxidation of water by an oxo-bridged ruthenium dimer. *J. Am. Chem. Soc.* **104,** 4029–4030 (1982).
3. Harriman, A., Pickering, I. J., Thomas, J. M. & Christensen, P. A. Metal-oxides as heterogeneous catalysts for oxygen evolution under photochemical conditions. *J. Chem. Soc. Faraday Trans. I* **84,** 2795–2806 (1988).
4. McDaniel, N. D., Coughlin, F. J., Tinker, L. L. & Bernhard, S. Cyclometalated iridium(III) aquo complexes: efficient and tunable catalysts for the homogeneous oxidation of water. *J. Am. Chem. Soc.* **130,** 210–217 (2008).

5. Hoertz, P. G., Kim, Y. I., Youngblood, W. J. & Mallouk, T. E. Bidentate dicarboxylate capping groups and photosensitizers control the size of IrO_2 nanoparticle catalysts for water oxidation. *J. Phys. Chem. B* **111,** 6845–6856 (2007).
6. Jiao, F. & Frei, H. Nanostructured cobalt oxide clusters in mesoporous silica as efficient oxygen-evolving catalysts. *Angew. Chem. Int. Ed.* **48,** 1841–1844 (2009).
7. Hara, M., Lean, J. T. & Mallouk, T. E. Photocatalytic oxidation of water by silica-supported *tris*(4,4′-dialkyl-2,2′-bipyridyl)ruthenium polymeric sensitizers and colloidal iridium oxide. *Chem. Mater.* **13,** 4668–4675 (2001).
8. Grätzel, M. Photoelectrochemical cells. *Nature* **414,** 338–344 (2001).
9. Fujishima, A. & Honda, K. Electrochemical photolysis of water at a semiconductor electrode. *Nature* **238,** 37–38 (1972).
10. Eisenberg, R. & Gray, H. B. Preface on making oxygen. *Inorg. Chem.* **47,** 1697–1699 (2008).
11. Kanan, M. W. & Nocera, D. G. *In situ* formation of an oxygen-evolving catalyst in neutral water containing phosphate and Co^{2+}. *Science* **321,** 1072–1075 (2008).
12. Turner, J. Oxygen catalysis: the other half of the equation. *Nature Mater.* **7,** 770–771 (2008).
13. Meyer, T. J. Catalysis—the art of splitting water. *Nature* **451,** 778–779 (2008).
14. Tagore, R., Crabtree, R. H. & Brudvig, G. W. Oxygen evolution catalysis by a dimanganese complex and its relation to photosynthetic water oxidation. *Inorg. Chem.* **47,** 1815–1823 (2008).
15. Grätzel, M. Light-induced charge separation and water cleavage in microheterogeneous aqueous systems. *Faraday Discuss.* **70,** 359–374 (1980).
16. Harriman, A., Nahor, G. S., Mosseri, S. & Neta, P. Iridium oxide hydrosols as catalysts for the decay of zinc porphyrin radical cations in water. *J. Chem. Soc. Faraday Trans. I* **84,** 2821–2829 (1988).
17. Nahor, G. S., Mosseri, S., Neta, P. & Harriman, A. Polyelectrolyte-stabilized metal-oxide hydrosols as catalysts for the photooxidation of water by zinc porphyrins. *J. Phys. Chem.* **92,** 4499–4504 (1988).
18. Gray, H. B. & Winkler, J. R. Long-range electron transfer. *Proc. Natl Acad. Sci. USA* **102,** 3534–3539 (2005).
19. Nam, K. T. *et al.* Virus-enabled synthesis and assembly of nanowires for lithium ion battery electrodes. *Science* **312,** 885–888 (2006).
20. Mao, C. B. *et al.* Virus-based toolkit for the directed synthesis of magnetic and semiconducting nanowires. *Science* **303,** 213–217 (2004).
21. Lee, Y. J. *et al.* Fabricating genetically engineered high-power lithium-ion batteries using multiple virus genes. *Science* **324,** 1051–1055 (2009).
22. Miller, R. A., Presley, A. D. & Francis, M. B. Self-assembling light-harvesting systems from synthetically modified tobacco mosaic virus coat proteins. *J. Am. Chem. Soc.* **129,** 3104–3109 (2007).
23. Lee, S. K., Yun, D. S. & Belcher, A. M. Cobalt ion mediated self-assembly of genetically engineered bacteriophage for biomimetic Co–Pt hybrid material. *Biomacromolecules* **7,** 14–17 (2006).
24. Glucksman, M. J., Bhattacharjee, S. & Makowski, L. Three-dimensional structure of a cloning vector. X-ray diffraction studies of filamentous bacteriophage M13 at 7 Å resolution. *J. Mol. Biol.* **226,** 455–470 (1992).
25. Fudickar, W. *et al.* Fluorescence quenching and size selective heterodimerization of a porphyrin adsorbed to gold and embedded in rigid membrane gaps. *J. Am. Chem. Soc.* **121,** 9539–9545 (1999).
26. Brixner, T. *et al.* Two-dimensional spectroscopy of electronic couplings in photosynthesis. *Nature* **434,** 625–628 (2005).
27. Nam, Y. S. *et al.* Virus-templated assembly of porphyrins into light-harvesting nanoantennae. *J. Am. Chem. Soc.* **132,** 1462–1463 (2010).
28. Morris, N. D., Suzuki, M. & Mallouk, T. E. Kinetics of electron transfer and oxygen evolution in the reaction of $[Ru(bpy)_3]^{3+}$ with colloidal iridium oxide. *J. Phys. Chem. A* **108,** 9115–9119 (2004).
29. Kim, J. W., Utada, A. S., Fernandez-Nieves, A., Hu, Z. B. & Weitz, D. A. Fabrication of monodisperse gel shells and functional microgels in microfluidic devices. *Angew. Chem. Int. Ed.* **46,** 1819–1822 (2007).
30. Soja, G. R. & Watson, D. F. TiO_2-catalyzed photodegradation of porphyrins: mechanistic studies and application in monolayer photolithography. *Langmuir* **25,** 5398–5403 (2009).

Acknowledgements

Y.S.N. would like to thank Y. Zhang for assistance with the scanning transmission electron microscopy, E.L. Shaw for help with the X-ray photoelectron spectroscopy, and K. Choi for experimental help and manuscript preparation. A.P.M thanks S. Cui for experimental help. This work was supported from Eni, S.p.A. (Italy) through the MIT Energy Initiative Program. We acknowledge the MIT Center for Materials Science and Engineering for use of microscopy and materials analysis facilities supported under grant no. DMR-9808941.

Author contributions

Y.S.N. designed the study, prepared samples, collected data, performed oxygen evolution analyses, analysed data and wrote the manuscript. A.P.M. helped design experiments and analyse data, built the oxygen analysis system and edited the manuscript. D.L. fabricated the virus microgels, optimized the fabrication processes, and edited the manuscript. J.W.K. suggested, designed and fabricated the virus microgels. D.S.Y. carried out the biopanning experiment. H.P. performed oxygen evolution analyses, scopoletin assays and ICP-AES analyses. T.S.P. performed biological experiments and edited the manuscript. D.A.W. supervised the microgel research and edited the manuscript. A.M.B. designed the study, supervised the overall work and edited the manuscript.

Additional information

The authors declare no competing financial interests. Supplementary information accompanies this paper at www.nature.com/naturenanotechnology. Reprints and permission information is available online at http://npg.nature.com/reprintsandpermissions/. Correspondence and requests for materials should be addressed to A.M.B.